Thickness-Independent Transport Channels in Topological Insulator Bi$_2$Se$_3$ Thin Films

Namrata Bansal,[1] Yong Seung Kim,[2,3] Matthew Brahlek,[2] Eliav Edrey,[2] and Seongshik Oh[2,*]

[1]*Department of Electrical and Computer Engineering, Rutgers, The State University of New Jersey, 94 Brett Road,
Piscataway, New Jersey 08854, USA*
[2]*Department of Physics & Astronomy, Rutgers, The State University of New Jersey, 136 Frelinghuysen Road,
Piscataway, New Jersey 08854, USA*
[3]*Graphene Research Institute, Sejong University, Seoul 143-747, South Korea*
(Received 26 August 2011; published 12 September 2012)

With high quality topological insulator Bi$_2$Se$_3$ thin films, we report thickness-independent transport properties over wide thickness ranges. Conductance remained nominally constant as the sample thickness changed from 256 to ~8 QL (where QL refers to quintuple layer, 1 QL ≈ 1 nm). Two surface channels of very different behaviors were identified. The sheet carrier density of one channel remained constant at ~3.0×10^{13} cm^{-2} down to 2 QL, while the other, which exhibited quantum oscillations, remained constant at ~8×10^{12} cm^{-2} only down to ~8 QL. The weak antilocalization parameters also exhibited similar thickness independence. These two channels are most consistent with the topological surface states and the surface accumulation layers, respectively.

Over the past few years, topological insulators (TIs) have emerged as an ideal platform for spintronics, quantum computations, and other applications [1–9]. They are predicted to have an insulating bulk state and spin-momentum-locked metallic surface states. This spin-momentum-locking mechanism and their band structure topology are predicted to prevent the surface metallic states from being localized. Among the TIs discovered so far, Bi$_2$Se$_3$ is considered one of the most promising because it has the largest bulk band gap of 0.3 eV and a well-defined single Dirac cone at the momentum zero point in k space [9]. Numerous reports have confirmed the presence of the topological surface states in this material [7,8,10–15]. However, its bulk state always turns out to be metallic instead of insulating, and so identifying the surface states in transport studies has been challenging. Although one obvious way to suppress the bulk conductance and sort out the surface contribution would be to make the sample thin until the surface contribution dominates; such a simple approach has so far evaded clear answers due to challenging material issues such as thickness- and environment-dependent bulk properties [13,16]. In this Letter, we report transport properties of a series of high quality Bi$_2$Se$_3$ thin films taken with well-controlled measurement protocols: we achieved dominant surface transport properties up to a few hundred nanometers in film thickness and identified two surface channels of different origins.

The Bi$_2$Se$_3$ films used for this study were grown on c-axis Al$_2$O$_3$ substrates ($10 \times 10 \times 0.5$ mm^3) with molecular beam epitaxy (MBE); the films were grown using the recently developed two-step scheme [17]; see Supplemental Material Sec. B [18]. The sharp reflection high energy electron diffraction pattern in Fig. 1(a) exhibits the high crystallinity of the film, and the atomically flat terraces

observed by atomic force microscopy in Fig. 1(b) are much larger than any previous reports on Bi$_2$Se$_3$ thin films [11,17,19,20], representing the high quality of these samples.

On these samples, transport measurements were made within 20 min of the sample being taken out of the MBE chamber in order to minimize the atmospheric doping effect [16]; see Supplemental Material Sec. A [18] for measurement details. Figure 2(a) shows that the resistance vs temperature (from 290 to 1.5 K) dependence is metallic down to ~30 K for all thicknesses 2–256 QL, where QL refers to quintuple layer. Below ~30 K the resistance remained almost constant, indicating static disorders as the dominant scattering mechanism, except for ultrathin films, which show slight resistance increase as temperature decreases. The first notable feature in Fig. 2(a) is that the
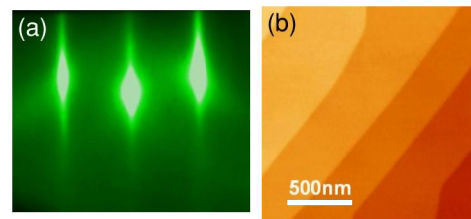

FIG. 1 (color online). Molecular beam epitaxy growth of Bi$_2$Se$_3$ films. (a) Reflection high energy electron diffraction pattern of a typical Bi$_2$Se$_3$ film grown on an Al$_2$O$_3$(0001) substrate by MBE. The sharp streaky pattern accompanied by the bright specular spot and Kikuchi lines is indicative of a high quality single crystalline growth. (b) 1.5×1.5 μm^2 scanned atomic force microscopy image of a 300 QL thick Bi$_2$Se$_3$ film grown on Al$_2$O$_3$(0001). Large terraces (largest ever reported for Bi$_2$Se$_3$ thin films) are observed, further verifying the high quality of the grown films.
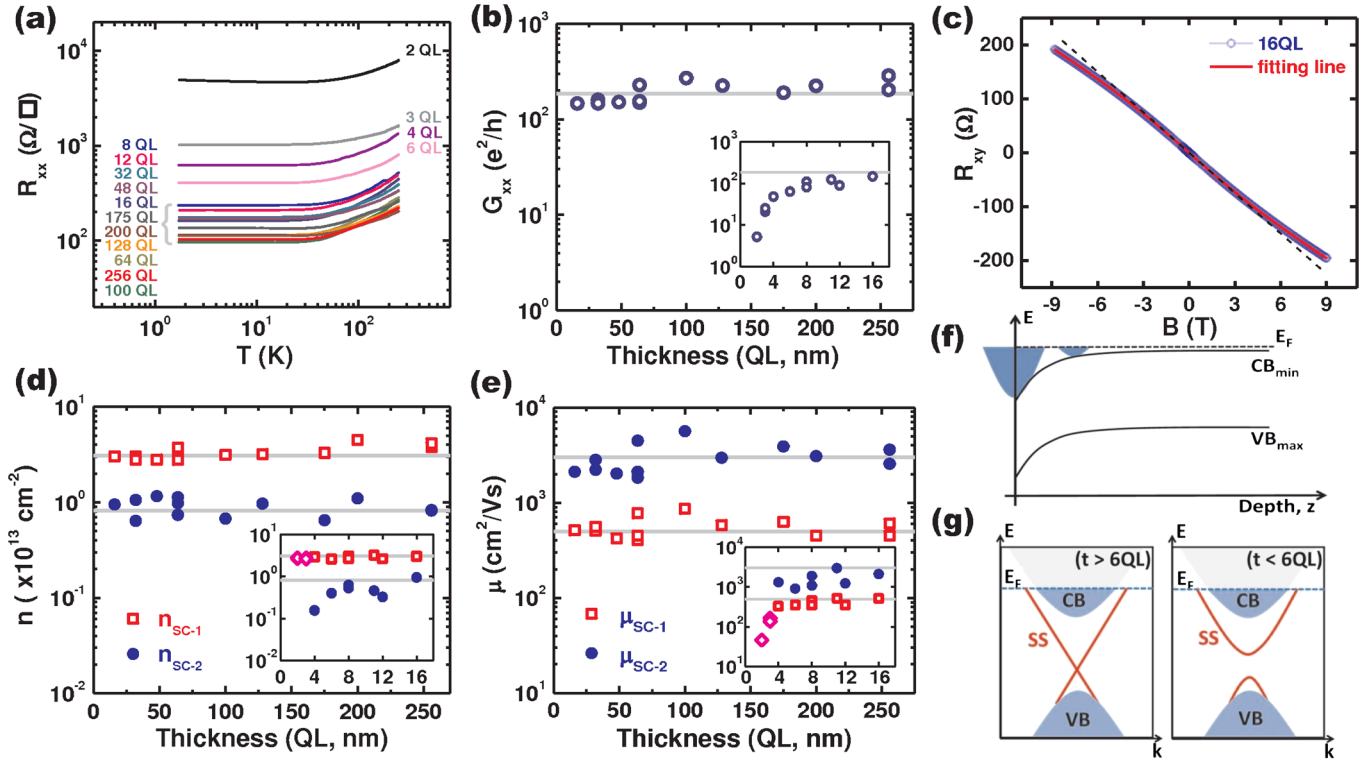
FIG. 2 (color online).   Transport properties of Bi_2Se_3 films. (a) Resistance vs temperature for each thickness. (b) Conductance at 1.5 K as a function of thickness. (c) Hall resistance vs magnetic field for a 16 QL sample plotted together with the two-carrier model fitting curve described in the text. (d) and (e) Sheet carrier densities and mobilities vs thickness. For 2 and 3 QL films (shown by a diamond in the inset), the sheet carrier density was directly read off from the linear R_{xy} vs B curve. In (b), (d), and (e), the horizontal straight lines are guides for illustration, and data for films thinner than 16 QL are plotted in the insets. (f) Conduction band minimum (CB_{min}) and valence band maximum (VB_{max}) along the depth of the sample, showing the downward band bending toward the surface. (g) Schematic surface band diagrams, depicting how the surface bands change through the critical thickness (6 QL) when the surface Fermi level is high: CB and SS stand for the bulk conduction band and the topological surface state, respectively.

low temperature resistance is quite thickness independent for samples between ~8 and 256 QL in thickness. This can be seen more clearly in the plot of conductance (G_{xx}) at 1.5 K versus sample thickness in Fig. 2(b). Within small error bars, G_{xx} is nominally constant for samples between ~8 and 256 QL thick. This observation suggests that the conductance in this thickness range is dominated by some surface transport channels.

The Hall effect measurement shown in Fig. 2(c) provides more insights regarding the origin of these surface channels. If all carriers had the same mobility, $R_{xy}(B)$ should appear as a straight line with the slope determined by $1/(n_{SC}e)$, with n_{SC} representing the total sheet carrier density. However, if there are multiple types of carriers with different but comparable mobilities, nonlinearty shows up in the $R_{xy}(B)$ data; if some carriers have much lower carrier densities or mobilities than others, they do not contribute to the nonlinearity of $R_{xy}(B)$ either. Therefore, the nonlinearity in Fig. 2(c) suggests the presence of multiple carrier types with comparable mobilities. Specifically, if two carrier types dominate the Hall effect, $R_{xy}(B)$ is given by $R_{xy}(B) = -(B/e)[(n_1\mu_1^2 + n_2\mu_2^2) +$

$B^2\mu_1^2\mu_2^2(n_1 + n_2)][(n_1\mu_1 + n_2\mu_2)^2 + B^2\mu_1^2\mu_2^2(n_1 + n_2)^2]^{-1}$, where n_1 and n_2 represent the two sheet carrier densities, μ_1 and μ_2 represent their respective mobilities, e is the electron charge, and B is the magnetic field. It turns out that this two-carrier model nicely fits all our Hall resistance data as shown in Fig. 2(c). This implies that the mobilities of all the significant conductance channels in our samples can be approximately grouped into two; in this model, carriers on opposite surfaces or on different bands will appear as part of the same channel if they have similar mobilities. In order to maximize the fitting reliability, we used the Hall conductance, $G_{xy}(B) \equiv -R_{xy}/(R_{xy}^2 + R_{xx}^2)$, instead of $R_{xy}(B)$ for the fitting and also reduced the number of fitting parameters to two by applying extra confinement from $G_{xx}(B)$; for details, see Supplemental Material Sec. C [18]. From this two parameter fitting, we extracted the four quantities, n_1, n_2, μ_1, and μ_2 for each sample.

The most notable feature in Fig. 2(d) is that one channel (n_{SC-1}) provided a nearly constant sheet carrier density of ~3.0×10^{13} cm^{-2} all the way down to 2 QL, whereas the other channel (n_{SC-2}) stayed at ~8×10^{12} cm^{-2} down to ~8 QL but gradually decreased for thinner samples.

This observation suggests first that a strong pinning mechanism exists for the surface Fermi level and that there exist two well-defined surface transport channels with different mobilities and thicknesses. Considering that angle-resolved photoemission spectroscopy (ARPES) studies consistently show that downward band bending develops on Bi_2Se_3 surfaces [see Fig. 2(f)] [21–24], not only the topological surface states but also the two-dimensional electron gas (2DEG) states in the quantum confined accumulation layers can be the sources of these surface channels. If we assume that only the lowest level of the 2DEG is filled (see Supplemental Material Sec. D [18] regarding this assumption), the sheet carrier densities (n_{SC}) of the topological surface state and the 2DEG should be given by $n_{SC,TI} = k_{F,TI}^2/(4\pi)$ and $n_{SC,2DEG} = k_{F,2DEG}^2/(2\pi)$, respectively, where k_F stands for the Fermi wave vectors and the factor of 2 difference is due to spin degeneracy. Because $k_{F,2DEG} < k_{F,TI}$, we should always have $n_{SC,2DEG} < 2n_{SC,TI}$. Therefore, with n_{SC-1} of $\sim 3.0 \times 10^{13}$ cm^{-2} and n_{SC-2} of $\sim 8 \times 10^{12}$ cm^{-2}, the inequality is satisfied only if n_{SC-1} is from the TI band and n_{SC-2} is from the 2DEG, but not the other way around. Moreover, when the thickness of the sample approaches that of the 2DEG, the confinement will start affecting the energy levels of the 2DEG. Because the film is confined by air on one side and sapphire substrate on the other, the thickness confinement can be well approximated by the simple infinite square potential well model. For the infinite well, the lowest energy level from the bottom of the conduction band is given by $h^2/(8m^*t^2)$, where h is the Planck constant, m^* is the effective electron mass, and t is the film thickness. With $m^* = 0.15m_e$ [22], where m_e is the bare electron mass, this level is found to be 0.04 eV for $t = 8$ nm and 0.6 eV for $t = 2$ nm. When compared with the typical band-bending energy of $0.1 \sim 0.3$ eV reported in ARPES studies [21–24], the 2DEG will start feeling the thickness effect by ~ 8 QL and will be severely affected by 2 QL. These analyses suggest that n_{SC-1}, which is constant down to 2 QL, is unlikely to originate from the 2DEG, whereas n_{SC-2}, which starts to change at ~ 8 QL, is more consistent with the expected behavior of a 2DEG; see Supplemental Material Secs. D and E for further discussion [18].

According to the standard TI theory, the thickness of a topological surface state [25] is ~ 1 nm, which is given by $\hbar\nu_F/E_g$, where ν_F ($= 4.5 \times 10^5$ m/s) is the Fermi velocity of the Bi_2Se_3 surface band and E_g ($= 0.3$ eV) is the bulk band gap of Bi_2Se_3 [8,26]; this implies that the thickness of the top and bottom surface states combined should be ~ 2 nm, which turns out to be exactly the thickness of the first channel, n_{SC-1}. If we assume that each of the top and bottom surfaces contribute equally to the observed carrier density of $\sim 3.0 \times 10^{13}$ cm^{-2}, $n_{SC,TI} = k_{F,TI}^2/(4\pi)$ provides $k_{F,TI}$ of 0.14 Å^{-1}, and this value is within the range that ARPES reports on band-bent Bi_2Se_3 samples [21–24]. There is a subtle point to discuss here,

though. It is known from an ARPES study that the Dirac point on the surface band disappears for films thinner than 6 QL [27]. However, if the surface Fermi level is far from the Dirac point, as depicted in Fig. 2(g), the sheet carrier density, which is simply a measure of k_F^2, should not be much affected by gap-opening at the Dirac point. Therefore, our observation of the constant sheet carrier density of the topological surface states down to 2 QL is not in contradiction with this gap-opening phenomenon at the Dirac point.

According to the above discussion, n_{SC-2} is likely from an ~ 8 nm thick surface 2DEG. If we assume symmetric band bending on both the top and bottom surfaces, the 2DEG corresponds to $n_{SC,2DEG}$ of $\sim 4 \times 10^{12}$ cm^{-2} on each surface with half the thickness. With $n_{SC,2DEG} = k_{F,2DEG}^2/(2\pi)$, this converts to $k_{F,2DEG}$ of 0.05 Å^{-1}. Interestingly, this Fermi wave vector is close to those obtained from Shubnikov–de Haas (SdH) oscillations of these samples; see Supplemental Material Sec. E for the details [18]. However, no SdH oscillations were observed around k_F of 0.14 Å^{-1}, the value associated with the topological surface band.

The mobilities in Fig. 2(e) also show thickness independence, within some error bars, down to $4 \sim 8$ QL. However, unlike n_{SC-1}, which remained constant down to 2 QL, its mobility, μ_{SC-1}, clearly degraded for ultrathin films. This difference can be understood by the fact that unlike the carrier density, which is simply a measure of the Fermi surface area, mobility is a measure of scattering time and thus susceptible to disorders and interactions, which is likely to become more significant for ultrathin samples. Another notable feature is that μ_{SC-1} is substantially smaller than μ_{SC-2} over the entire thickness range. This observation may look puzzling according to the common expectation that the mobility of the topological surface band should be high due to absence of backscattering. However, this expectation should be taken with caution. First of all, the topological protection mechanism guarantees only the metallicity of the surface state, and the mobility should still depend on the details of interactions. Second, considering that backscattering accounts for only a small fraction of the scattering [4] and that the topological surface state is spatially more confined than the 2DEG, there is no fundamental reason that the topological surface state should have a higher mobility than the 2DEG. Because high mobility ($\mu \gg 1/B$) is critical for the observation of SdH oscillations, we may or may not observe SdH oscillations from any of these surface channels, even if both are metallic. With $\mu_{SC-1} \approx 0.05$ m^2 V^{-1} s^{-1}, $\mu_{SC-2} \approx 0.3$ m^2 V^{-1} s^{-1}, and $B_{max} = 9$ T, we get $\mu_{SC-1}B_{max} \approx 0.5$ and $\mu_{SC-2}B_{max} \approx 3$. According to these numbers, we expect some SdH oscillations from SC-2 (2DEG) but none from SC-1 (topological surface band), and this expectation is experimentally confirmed in Supplemental Material Sec. E [18].
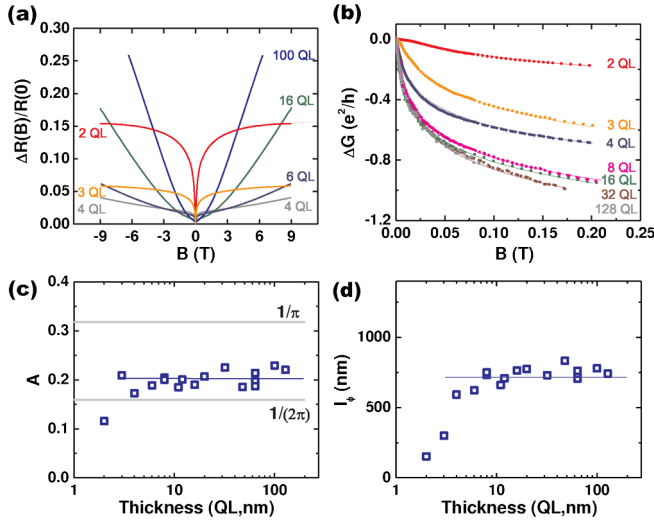
FIG. 3 (color online). Weak antilocalization effect. (a) Normalized resistance change as a function of the magnetic field, measured at 1.5 K, where $\Delta R(B) \equiv R(B) - R(0)$. The deep cusp in low field regime is characteristic of the WAL effect. (b) Conductance change vs magnetic field in the low field regime: 8–128 QL curves are almost overlapping. The theoretical WAL fitting curves are plotted together for each data set. (c) and (d) The WAL fitting parameters, A and l_φ, vs the thickness, respectively. The horizontal lines are a guide for illustration.

Figure 3 presents another set of thickness-independent transport properties. In the normalized resistance vs magnetic field data in Fig. 3(a), the cusp around the zero magnetic field is an indication of the weak antilocalization (WAL) effect. Although Fig. 3(a) gives the impression that the magneto-transport is highly thickness dependent, the small magnetic field regime in Fig. 3(b) provides a surprisingly simple picture. On the surface of TI materials, backscattering is, at the minimum, due to time-reversal symmetry when the magnetic field is absent. With an increasing magnetic field, which breaks the time-reversal symmetry, backscattering increases and leads to a reduction in conductance as in Fig. 3(b); this phenomenon is called the WAL effect [13,14]. Just like the other transport properties, this WAL effect also shows thickness independence for films thicker than ~8 QL. According to the standard WAL theory [28], the 2D magnetoconductance $G(B)$ is expected to change as $\Delta G(B) = A(e^2/h)[\ln(B_\phi/B) - \Psi(1/2 + B_\phi/B)]$, where A is a coefficient predicted to be $1/(2\pi)$ for each 2D channel, B_ϕ is the dephasing magnetic field, and $\Psi(x)$ is the digamma function. The dephasing magnetic field is related to the phase coherence length l_ϕ via $B_\phi = \hbar/(4el_\phi^2)$ [13,14].

Figure 3(c) shows that A remains almost constant from 3 through 128 QL, with a value between $1/(2\pi)$ and $1/\pi$. If the top and bottom surfaces were completely decoupled from each other with an insulating bulk state, A should be close to $1/\pi$. On the other hand, if the bulk of the film dominates and/or the bulk and two surfaces behave as a strongly coupled single entity, then the value should reduce to $1/(2\pi)$ [13].

Figure 3(c) shows that our films are somewhere between these two extremes. However, if the bulk contribution to the WAL effect were significant, l_ϕ should grow with thickness [13]. Therefore, l_ϕ being almost thickness-independent between ~8 and 128 QL in Fig. 3(d) is a clear indication that the observed WAL effect originates mainly from surface channels [13].

In summary, significant advances in Bi_2Se_3 thin film qualities allowed observation of dominant, thickness-independent surface transport channels. Conductance, sheet carrier densities, mobilities, and WAL parameters remained nearly independent of thickness over two orders of the thickness range. Such thickness-independent transport properties, trivially expected in TIs, were never observed before because of nontrivial bulk effects. In order to explain the observed surface transport properties, not only the topological surface states but also the quantum confined 2DEG channels have to be considered. How each of these different surface channels responds against various excitations is an important scientific and technological question that needs to be further investigated in future studies.

*ohsean@physics.rutgers.edu
[1] M. Z. Hasan and C. L. Kane, Rev. Mod. Phys. **82**, 3045 (2010).
[2] X. L. Qi and S. C. Zhang, Phys. Today **63**, No. 1, 33 (2010).
[3] J. E. Moore, Nature (London) **464**, 194 (2010).
[4] P. Roushan, J. Seo, C. V. Parker, Y. S. Hor, D. Hsieh, D. Qian, A. Richardella, M. Z. Hasan, R. J. Cava, and A. Yazdani, Nature (London) **460**, 1106 (2009).
[5] Y. L. Chen, J. G. Analytis, J. H. Chu, Z. K. Liu, S. K. Mo, X. L. Qi, H. J. Zhang, D. H. Lu, X. Dai, Z. Fang, S. C. Zhang, I. R. Fisher, Z. Hussain, and Z. X. Shen, Science **325**, 178 (2009).
[6] D. Hsieh, Y. Xia, L. Wray, D. Qian, A. Pal, J. H. Dil, J. Osterwalder, F. Meier, G. Bihlmayer, C. L. Kane, Y. S. Hor, R. J. Cava, and M. Z. Hasan, Science **323**, 919 (2009).
[7] H. L. Peng, K. J. Lai, D. S. Kong, S. Meister, Y. L. Chen, X. L. Qi, S. C. Zhang, Z. X. Shen, and Y. Cui, Nature Mater. **9**, 225 (2010).
[8] Y. Xia, D. Qian, D. Hsieh, L. Wray, A. Pal, H. Lin, A. Bansil, D. Grauer, Y. S. Hor, R. J. Cava, and M. Z. Hasan, Nature Phys. **5**, 398 (2009).
[9] H. J. Zhang, C. X. Liu, X. L. Qi, X. Dai, Z. Fang, and S. C. Zhang, Nature Phys. **5**, 438 (2009).
[10] T. Hanaguri, K. Igarashi, M. Kawamura, H. Takagi, and T. Sasagawa, Phys. Rev. B **82**, 081305 (2010).
[11] P. Cheng, C. L. Song, T. Zhang, Y. Y. Zhang, Y. L. Wang, J. F. Jia, J. Wang, Y. Y. Wang, B. F. Zhu, X. Chen, X. C.

Ma, K. He, L. L. Wang, X. Dai, Z. Fang, X. C. Xie, X. L. Qi, C. X. Liu, S. C. Zhang, and Q. K. Xue, Phys. Rev. Lett. **105**, 076801 (2010).

[12] J. G. Analytis, R. D. McDonald, S. C. Riggs, J.-H. Chu, G. S. Boebinger, and I. R. Fisher, Nature Phys. **6**, 960 (2010).

[13] Y. S. Kim, M. Brahlek, N. Bansal, E. Edrey, G. A. Kapilevich, K. Iida, M. Tanimura, Y. Horibe, S.-W. Cheong, and S. Oh, Phys. Rev. B **84**, 073109 (2011).

[14] J. Chen, X. Y. He, K. H. Wu, Z. Q. Ji, L. Lu, J. R. Shi, J. H. Smet, and Y. Q. Li, Phys. Rev. B **83**, 241304 (2011).

[15] R. Valdés Aguilar, A. V. Stier, W. Liu, L. S. Bilbro, D. K. George, N. Bansal, L. Wu, J. Cerne, A. G. Markelz, S. Oh, and N. P. Armitage, Phys. Rev. Lett. **108**, 087403 (2012).

[16] M. Brahlek, Y. S. Kim, N. Bansal, E. Edrey, and S. Oh, Appl. Phys. Lett. **99**, 012109 (2011).

[17] N. Bansal, Y. S. Kim, E. Edrey, M. Brahlek, Y. Horibe, K. Iida, M. Tanimura, G.-H. Li, T. Feng, H.-D. Lee, T. Gustafsson, E. Andrei, and S. Oh, Thin Solid Films **520**, 224 (2011).

[18] See Supplemental Material at http://link.aps.org/supplemental/10.1103/PhysRevLett.109.116804 for growth and measurement details, fitting procedure, band-bending discussion, and SdH oscillation analysis.

[19] H. D. Li, Z. Y. Wang, X. Kan, X. Guo, H. T. He, Z. Wang, J. N. Wang, T. L. Wong, N. Wang, and M. H. Xie, New J. Phys. **12**, 103038 (2010).

[20] A. Richardella, D. M. Zhang, J. S. Lee, A. Koser, D. W. Rench, A. L. Yeats, B. B. Buckley, D. D. Awschalom, and N. Samarth, Appl. Phys. Lett. **97**, 262104 (2010).

[21] C. Chen, S. He, H. Weng, W. Zhang, L. Zhao, H. Liu, X. Jia, D. Mou, S. Liu, J. He, Y. Peng, Y. Feng, Z. Xie, G. Liu, X. Dong, J. Zhang, X. Wang, Q. Peng, Z. Wang, S. Zhang, F. Yang, C. Chen, Z. Xu, X. Dai, Z. Fang, and X. J. Zhou, Proc. Natl. Acad. Sci. U.S.A. **109**, 3694 (2012).

[22] J. G. Analytis, J. H. Chu, Y. L. Chen, F. Corredor, R. D. McDonald, Z. X. Shen, and I. R. Fisher, Phys. Rev. B **81**, 205407 (2010).

[23] M. Bianchi, D. Guan, S. Bao, J. Mi, B. B. Iversen, P. D. C. King, and P. Hofmann, Nature Commun. **1**, 128 (2010).

[24] P. D. C. King, R. C. Hatch, M. Bianchi, R. Ovsyannikov, C. Lupulescu, G. Landolt, B. Slomski, J. H. Dil, D. Guan, J. L. Mi, E. D. L. Rienks, J. Fink, A. Lindblad, S. Svensson, S. Bao, G. Balakrishnan, B. B. Iversen, J. Osterwalder, W. Eberhardt, F. Baumberger, and P. Hofmann, Phys. Rev. Lett. **107**, 096802 (2011).

[25] J. Linder, T. Yokoyama, and A. Sudbø, Phys. Rev. B **80**, 205401 (2009).

[26] D. Hsieh, Y. Xia, D. Qian, L. Wray, J. H. Dil, F. Meier, J. Osterwalder, L. Patthey, J. G. Checkelsky, N. P. Ong, A. V. Fedorov, H. Lin, A. Bansil, D. Grauer, Y. S. Hor, R. J. Cava, and M. Z. Hasan, Nature (London) **460**, 1101 (2009).

[27] Y. Zhang, K. He, C. Z. Chang, C. L. Song, L. L. Wang, X. Chen, J. F. Jia, Z. Fang, X. Dai, W. Y. Shan, S. Q. Shen, Q. A. Niu, X. L. Qi, S. C. Zhang, X. C. Ma, and Q. K. Xue, Nature Phys. **6**, 584 (2010).

[28] S. Hikami, A. Larkin, and Y. Nagaoka, Prog. Theor. Phys. **63**, 707 (1980).